International Journal on
"Technical and Physical Problems of Engineering"
(IJTPE)
Published by International Organization of IOTPE

ISSN 2077-3528
IJTPE Journal
www.iotpe.com
ijtpe@iotpe.com

March 2014 | Issue 18 | Volume 6 | Number 1 | Pages 46-55

DESCRIPTION OF CHARACTERISTICS OF THE CHARGE TRANSFER WITHIN SOLID INSULATING MATERIALS

A. Ganjovi S. Khezripour

Photonics Research Institute, Institute for Science and High Technology and Environmental Sciences, Graduate University of Advanced Technology, Kerman, Iran, ganjovi@icst.ac.ir, saeedeh1363@gmail.com

Abstract- In this paper, the numerical calculations of spatiotemporal characteristics of the charge transfer within solid insulating materials are performed by means of a two dimensional axisymmetric model. The solid dielectric material is supposed to be a non-ideal polyethylene. In this model, the continuity equations for fluxes of charge carriers are coupled with Poisson's equation for computing electric fields affected by temporal and spatial variations of space charges in the dielectric material. An efficient stabilized finite element method for solving of these equations is represented, which provides wiggle free solutions without introducing much artificial diffusion. It was seen that the conductivity under applied electric field decreases over time. The electric field shows higher effects on the net charge density at positions nearer to the anode and the density of the charged species are higher at positions close to the both electrodes. The dependence of the charge transfer process on the amplitude of the applied electric field, solid dielectric dimensions and temperature is analyzed. In order to verify the model, the obtained results are compared with the existing experimental and simulation data, whenever possible.

Keywords: Solid Insulating Materials, Space Charge Transport.

I. INTRODUCTION

Charge transport within solid dielectric materials is an undesirable phenomenon and potentially leads to unrecoverable damages of an insulation system [1, 2]. Different situations can be observed when analyzing time and space evolution of charge carriers depending upon the orientation of the dielectric in the applied field [3]. Generally, the presence of space charges within the bulk of insulation or even at insulation electrode interfaces can affect considerably the electric field distribution.

Therefore, initially, an electric field concentration can locally induce accelerated damage and consequently it is able to trigger early insulation breakdown [4]. It is almost clear that the transport of space charges within solid dielectric materials may play a considerable role in weakening polymeric insulation. In related existing literature, the different possible scenarios of degradation mechanisms, thermally activated, but accelerated by the presence of space charges, are examined [5].

The problems of charge transport through dielectric materials are extensively studied in single and double injection cases, the spreading of charge packets, and the coupling of transport and dipolar responses [6-9]. Roy et al. used a specially developed pulsed electro acoustic apparatus low density polyethylene films under a high DC electric field and measured the electroluminescence and Space Charge (SC) distribution in bulk of solid dielectric material. Moreover, with the help of a numerical model of transport including the effect of charge trapping and recombination, they interpreted the observed behaviors of space charges [3].

Roy et al. introduced some numerical methods pertaining to the simulation of charge transport in solid dielectrics that are generally scattered over numerical analysis and computing literature [10]. They considered an example of a set of physical parameters needed to describe charge transport and introduced mathematical equations that must be solved [10]. Depending upon the orientation of the solid insulating dielectric in the applied field, space charged carriers show different situations.

The present study will concentrate on temporal and spatial evolution of conductivity of solid dielectric material between two parallel plate electrodes along with other parameters. Thus, it will be shown that the charge transfer occurs mostly due to the axial (normal to the parallel plate electrodes surface) component of the electric field. Thus, charge transfer occurs mostly due to the axial (normal to the surface) component of the field. Such an arrangement is typical for barrier discharges [11].

The presented computer model is based on space charge formation and transfer process in a non-ideal solid dielectric material between parallel plate circular metallic electrodes. The material considered is polyethylene (PE). This computational model used to describe these phenomena takes the following physical parameters and processes into consideration: charge deposition profiles, charge drift due to a finite carrier mobility, deep trapping without release, and trap filling due to a finite trap density. Recombination processes involving mobile and trapped carriers are taken into account.

Temporal and spatial evolution of space charge formation and transfer such as charged carries densities in dielectric media and conductive properties of polyethylene

are taken into account. Moreover, the effects of external parameters such as amplitude of the applied electric field, solid dielectric dimensions on charge transfer process are investigated. A finite element method based on Galerkin formulation of governing equations for the charge transport phenomena inside solid dielectric materials is applied. This method is powerful for these equations as they include non-smooth coefficient functions.

Moreover, the convergence order can easily be improved by increasing the polynomial degree of the basic functions. Therefore, this powerful stabilized finite element method is applied to model to describe the main features of the space and time dependent behavior of the particles, the mean electron energy, and the electric potential inside solid dielectric material dominated by highly non-uniform electric fields due to space charge effects [12-14].

II. SIMULATION MODEL

A sample of a solid dielectric material is assumed to be placed between two parallel plate circular metallic electrodes. The cathode was located at the origin of the axial coordinate $z = 0$, and the anode was on the distance S_z from the cathode, as shown in the Figure 1. The theoretical description of charge transport in this solid dielectric material is based on a 2D simulation model with rotational symmetry, which is similar to the simulation model presented in the reference [11]. In this model, the dimensionality of the computer model could be reduced to a quasi three dimensional case which is a 2D simulation model with rotational symmetry.

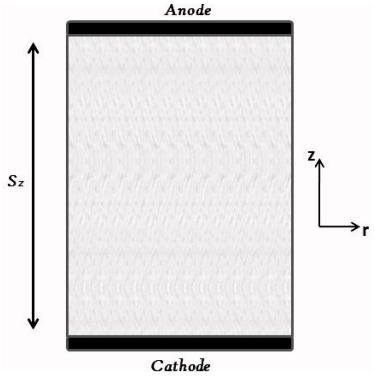

Figure 1. Geometry of sample of a solid dielectric material [11]

When, due to internally generated carrier pairs, conduction occurs, there are at least two active species, and one of them or both may move. However, injection of one sign or of both signs of carrier may also occur. Single carrier transport might be characterized by some parameters such as energy barriers to injection and extraction, mobility, perhaps activation energy for transport, a trap density, a trap energy depth, a capture cross section, and a free carrier lifetime for deep trapping [15]. In this model, it has been assumed that the charged carriers are provided only by injection at the electrodes.

Transport of charged carriers through shallow levels in solid dielectric materials is related to the structural disorder of the insulating material. Therefore, the conduction in the solid dielectric material would be due to a constant effective mobility. Moreover, It was assumed that the insulating material is not a perfect insulator, so its bulk conductivity σ is due to hopping of charge carriers between localized states (traps) and it is determined by the effective mobility of their carriers [11].

The presented model is based on the continuity condition in terms of electrons and holes densities combined with the equations for the densities of charges trapped in deep traps as well as Poisson's equation material in order to determine electrostatic field within solid dielectric as follows [11]:

$$\begin{cases} \partial n_e/\partial t = \nabla.(n_e \mu_e E + D_e \nabla n_e) - \\ -R_{eht} n_e n_{ht} - R_{eh} n_e n_h - \\ -T_e n_e (1 - n_{et}/n_{et}^0) + \nu n_{et} \exp(\varphi_{etr}/k\theta)\left(n_{et}/n_{et}^0\right) \end{cases} \quad (1)$$

$$\begin{cases} \partial n_h/\partial t = \nabla \cdot (n_h \mu_h E + D_h \nabla n_h) - \\ -R_{eht} n_e n_{ht} - R_{eh} n_e n_h - \\ -T_h n_h (1 - n_{ht}/n_{ht}^0) + \nu n_{ht} \exp(\varphi_{etr}/k\theta)\left(n_{ht}/n_{ht}^0\right) \end{cases} \quad (2)$$

$$\begin{cases} dn_{et}/dt = -R_{eth} n_{et} n_h - R_{etht} n_{et} n_{ht} - \\ -T_e n_e (1 - n_{et}/n_{et}^0) + \nu n_{et} \exp(\varphi_{etr}/k\theta)\left(n_{et}/n_{et}^0\right) \end{cases} \quad (3)$$

$$\begin{cases} dn_h/dt = -R_{eht} n_e n_{ht} - R_{eth} n_e n_{ht} - \\ -T_h n_h (1 - n_{ht}/n_{ht}^0) + \nu n_{ht} \exp(\varphi_{etr}/k\theta)\left(n_{ht}/n_{ht}^0\right) \end{cases} \quad (4)$$

$$\nabla \cdot (\varepsilon \nabla V) = -\rho = -e(n_h + n_{ht} - n_e - n_{et}) \quad (5)$$

where, n_e, n_h, n_{et} and n_{ht} are densities of electrons, holes, trapped electrons and trapped holes, respectively. R_{eht}, R_{eth}, R_{eh}, and R_{etht} are stands for recombination coefficients between mobile electrons and trapped holes, trapped electrons and mobile holes, mobile electrons and holes and trapped electrons and trapped holes, respectively. In addition, T_e and T_h are trapping coefficients for electrons and holes, respectively, ν is the attempt to escape frequency, φ_{etr} and φ_{htr} are barrier heights for de-trapping of electrons and holes, respectively. V, ρ and ε ($= \varepsilon_0\varepsilon_r$) are the potential across solid dielectric material, net charge density and the permittivity of the solid dielectric material.

Methods to solve Poisson's equation, which is an elliptic equation via finite differences, are compared and contrasted by Hockney et al [16]. The methods are including iterative techniques and direct matrix inversions. Among the fastest methods is a direct matrix inversion called cyclic reduction. Unlike Fourier transform methods, cyclic reduction may easily be generalized to cylindrical and spherical coordinate systems. Unfortunately, like Fourier transform methods, cyclic reduction requires that the potential equation be separable. Generally, the Equation (5) is not separable and cyclic reduction cannot be used. Instead, we choose a more general, but somewhat slower, method to solve this equation, which is based on iterative techniques.

In many models, this computational inefficiency, owing to its advantages, is ignorable. Then, the used method is Dynamic Alternating Direction Implicit (DADI) method, which is an iterative technique devised by Doss et

al [17] that converges rapidly for equations similar to Equation (5). According to Doss et al, DADI is a factor of 4 slower than a fast direct matrix inversion method for solving Equation (5) and the directional splitting in the scheme makes DADI easily vectorized for large simulations done on vector computers.

Hewett et al [18], applied a variation of the method to solve a coupled set of elliptic equations arising from a reduced version of Maxwell's equations, and their solutions required much less computer time than the bi-conjugate gradient method previously used [19]. DADI adds an artificial time dependence to convert Equation (5) into a parabolic equation as follows [17]:

$$\frac{\partial V}{\partial t} = \nabla.[\varepsilon(z,r)\nabla V] + \rho \tag{6}$$

Then non-iterative ADI is used to advance the parabolic equations in time '*t'*. This parabolic equation is then solved along with Equations (1) to (4). DADI and other iterative techniques are usually used to solve for steady state problems in which the time derivatives approach zero.

The components of the current density flowing between electrodes in solid dielectric media due to the applied electric field $E(z,r,t)$ are as follows [10]:

$$J_e(z,r,t) = e\mu_e n_e(z,r,t)E(z,r,t) \tag{7}$$

$$J_h(z,r,t) = e\mu_h n_h(z,r,t)E(z,r,t) \tag{8}$$

where, n_e and n_h are densities of electrons and holes, respectively. The total current density, $J_{total}(z,r,t)$ is obtained from Maxwell-Ampere equation that is:

$$J_{total}(z,r,t) = J(z,r,t) + \varepsilon\,\partial E(z,r,t)/\partial t \tag{9}$$

where, the first term on right hand side is the conduction contribution ($J_e(z,r,t) + J_h(z,r,t)$) and the second term is the displacement current [10]. Negative and positive charges appear in the bulk of the material due to injection from the electrodes that is described by Schottky's law [11]:

$$J_e(0,r,t) = AT^2 \exp(-\frac{e\phi_c}{kT}).\exp(-\frac{e}{kT}\sqrt{\frac{eE(0,r,t)}{4\pi\varepsilon}}) \tag{10}$$

$$J_h(S_z,r,t) = AT^2 \exp(-\frac{e\phi_a}{kT}).\exp(-\frac{e}{kT}\sqrt{\frac{eE(0,r,t)}{4\pi\varepsilon}}) \tag{11}$$

where, $J_e(0,r,t)$ and $J_h(S_z,r,t)$ are the electronic components of the current density injected from the cathode the current density at the anode due to injected holes respectively. φ_c and φ_a are the injection barriers for the cathode and anode materials, respectively and $E(0,r,t)$ and $E(S_z,r,t)$ stand for the electric field strength at cathode and anode surfaces, respectively [11].

In this work, the properties of the solid dielectric material such as charged carrier densities, and electric current and potential are assumed to be continuous with respect to space and time. Thus, a stabilization is achieved by means of a modification of the basic functions of the test space [12-14]. The resulting finite element method has proved to be applicable to model time dependent, spatially two dimensional of the charge transport phenomena inside solid dielectric materials.

To solve the set of coupled Equations (1) to (4) and (6), a stabilized finite element method has been adapted. Based on [12-14], an upwind Petrov-Galerkin finite element method (PGFEM) has been used to achieve a stabilized spatial discretization of continuity Equations (1) and (2) of charged particles and the Poison's equation with artificial time dependence where significant contributions of the first spatial derivatives can occur. This method takes into account the exponential approximation of Scharfetter and Gummel [20] for discretization of Equations (1) and (2) and (6) as well as second order standard finite difference approximation of the spatial derivatives of these equations.

The solution of nonlinear coupled set of Equations (1) to (4) and (6) with the spatial grid spacing 'h' and the time step Δt for each time step is obviated by applying the following time stepping scheme on the discrete space time mesh [20]:

$$\begin{cases} r_i = ih_r, & i = 0,\cdots,M_r \\ z_j = jh_z, & j = 0,\cdots,M_z \\ t_k = k\Delta t, & k = 0,\cdots,N \end{cases} \tag{12}$$

For all $k = 0, ..., N$-1, the discrete representation of the continuity Equation (1) to (4) and (6) in time as follows:

$$\left.\begin{array}{l} (n_e)_{i,j}^{k+1} = n_e(z_j, r_i, t_{k+1}) \\ (n_h)_{i,j}^{k+1} = n_h(z_j, r_i, t_{k+1}) \\ (V)_{i,j}^{k+1} = V(z_j, r_i, t_{k+1}) \\ (n_{et})^{k+1} = n_{et}(t_{k+1}) \\ (n_{ht})^{k+1} = n_{ht}(t_{k+1}) \end{array}\right\} \text{for} \begin{cases} i = 1,\ldots M_r \\ \text{and} \\ j = 1,\ldots M_z \end{cases} \tag{13}$$

where, the unknown densities at the time t^{k+1} are on the right hand side of these equations [20].

Table 1. Simulation data [11]

Symbols		Value
Band mobilities, μ_b, cm^2/Vs	For electrons	8×10^{-13}
	For holes	4×10^{-12}
Depths of shallow traps, eV		0.05
Diffusion coefficient, $D_{e,h}$, cm^2/s	$D_{e,h} = (kT/e).\ \mu_{e,h}$	
Recombination coefficients, cm^3/s	R_{eht}	1.6×10^{-27}
	R_{eth}	3.2×10^{-26}
	R_{eh}	0
	R_{etht}	4.8×10^{-26}
Densities of deep traps, cm^{-3}	For electrons	6.25×10^{14}
	For holes	9.375×10^{14}
Trapping coefficients, T_e, T_h, s^{-1}	For electrons	10^{-3}
	For holes	2×10^{-3}
Attempt to escape frequency, ν, s^{-1}		6×10^{12}
Barrier height for de-trapping, eV	For electrons	1.05
	For holes	1.05
Barrier height for injection, eV	For electrons (φ_c)	1.25
	For holes (φ_a)	1.23
Material dielectric constant, ε_r		2.3
Temperature, T, K		293
Applied Electric Field, kV/mm	E_a	100

In the other hand, a numerical treatment of the Equations (1), (2) and (6) in space domain, i.e. (z,r), by means of finite element methods based on the associated weak formulation has been derived. Therefore, an appropriate trial space $\mathcal{U} \subset \mathcal{H}^1$ and test space $\mathcal{V} \subset \mathcal{H}^1$ has to be specified for each equation, where $\mathcal{H}^1$ denotes the space of functions which are square integrable on the interval $[0, S_z]\times[0, R]$ together with their weak derivatives. A complete discussion on this scheme is available in the presented work by Becker et al [21]. The boundary conditions in Hilbert spaces are defined as follows [21]:

$$\upsilon^e = \upsilon^h = \upsilon^{pot} = \{v \in \mathcal{H}^1 \mid v(0,r) = v(S_z,\ r) = 0\},$$
$$u^e = \{v \in \mathcal{H}^1 \mid v(0,r) = [\text{from Equations } (7) \text{ and } (10)]\},$$
$$v(S_z,\ r) = J_e(S_z,\ r,\ t)/e\mu_e E(S_z,\ r,\ t)\}, \quad (14)$$
$$u^h = \{v \in \mathcal{H}^1 \mid v(0,r) = J_h(0,r,t)/e\mu_h E(0,r,t), v(S_z,r) =$$
$$= [\text{from Equations } (8) \text{ and } (11)]\},$$
$$u^{pot} = \{v \in \mathcal{H}^1 \mid v(0,r) = 0,\ v(S_z,\ r) = V_a\}$$

Moreover, the Neumann conditions were used for all densities and for the electric potential on symmetry axis (r = 0) and on the outer boundary of the domain (r = R).

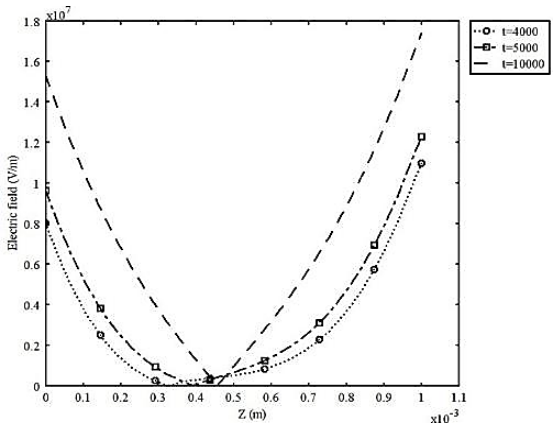

Figure 2. Electric field distribution in 1 mm sample from cathode to the anode at different moments of time after voltage application

III. RESULTS AND DISCUSSIONS

The presence of space charge inside the solid dielectric causes distortions in electric field distribution in the solid dielectric and may affect the lifetime of the electrical line. The model describes injection, transport, and trapping. Results are presented here with simulation parameters presented in Table 1 [11]. When an electric field is applied to the solid dielectric material, reorganization of molecular chains in amorphous regions will take place due to induced mechanical stress. Figure 2 shows the electric field across a 1mm sample of polyethylene (PE) as a function of z (distance from the cathode) at different moments of time.

The resulting electric field distribution indicates field reduction from the cathode electrode towards anode electrode. On the other hand, Figure 3 shows the net charge density ($\rho = e\ (n_h + n_{ht} - n_e - n_{et})$) as a function of distance from the cathode (z) and different moments of time after voltage application. The absolute value of net charge density at the positions near to both electrodes is higher. The observed trend in the variations of net charge density is similar to the reported results in the some literatures [22-27], such as the experimental works by Zhou et al. [28]. They measured net space charge distribution within a solid dielectric material (Kapton®500HN) under various aging temperatures and immediately after short circuiting.

They observed that the hetero charges are trapped near both electrodes and consequently the net charge density is higher in these regions. They stated that the Hetero charge increases the electric field near the electrodes and this will be helpful in the charge injection process from the electrodes. In the other hand, the net charge density is seen to reduce to zero and even negative values. Away from the anode and cathode, the variation in net charge density is almost similar at all moments of time, while the magnitudes are different.

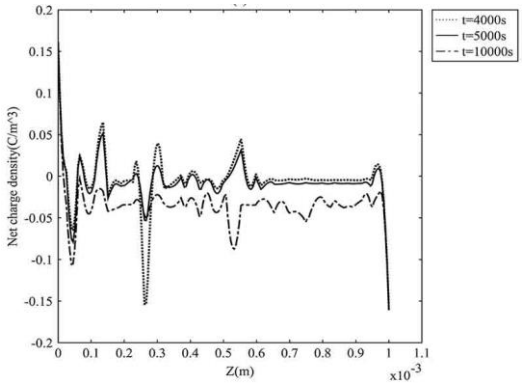

Figure 3. Net charge density distribution in 1 mm sample versus distance from cathode at different moments of time after voltage application

Therefore, reduction in the electric field is due to the lower amounts of charged carriers in the bulk of solid dielectric material. The observed behavior of electric field is in agreement with the findings by Serdyuk et al. [11] for modeling of a sample solid dielectric material of 100 μm length after a voltage application that shows a decrease in electric field along z-axis next to the cathode, which is followed by an increase next to the anode. It should be mentioned that the electric field close to the cathode is a little lower than the positions close to the anode. This is due to more number of negatively charged carriers injected from the cathode electrode in compared with anode electrode into solid dielectric material, which has more lowering effects on the applied field.

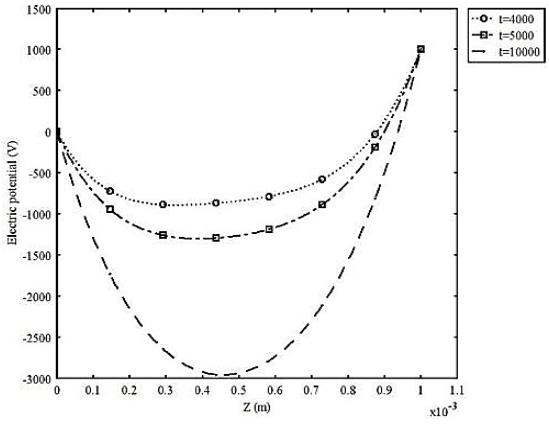

Figure 4. Electric potential distribution in 1 mm sample at different moments of time after voltage application

To complement the discussions on electric field across the solid dielectric material, the spatial variation of electric potential (E = grad V) at different moments of time are presented in Figure 4. The results are presented for three different positions along z-axis in solid dielectric material. It almost shows similar temporal variations for different positions. As is shown, the variations in the electric potential at lower steps of time (t = 4000 s) is lower.

Due to increased ionization, at the next time steps, the variation on the electric potential across the solid dielectric material increases. The variation of electric potential across the solid dielectric material appears to follow the variation of electric field (E) which is presented in Figure 2. However, the effect of electric field on the net charge density is higher at positions nearer to the anode, obviously due to greater ionization of traps in this region.

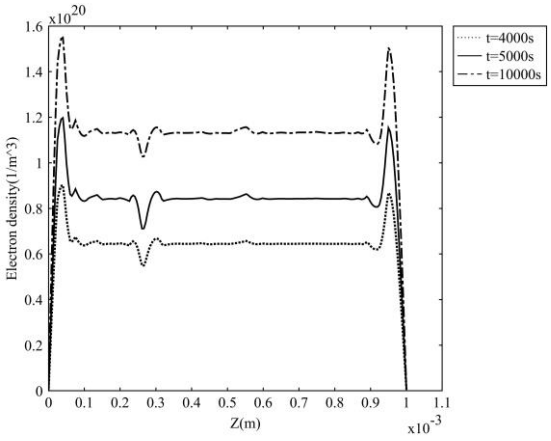

(a)

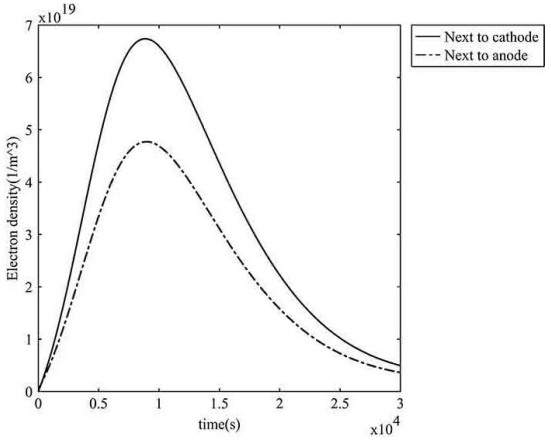

(b)

Figure 5. Electron density in the PE obtained from the simulations for a 1 mm sample, (a) versus distance from the cathode at different moments of time and, (b) versus time at the positions close to cathode (r = 0, z = 0.01 mm) and anode (r = 0, z = 0.99 mm) after voltage application

This axisymmetric model helps to understand the dynamic behavior of space charge inside the solid dielectric material. Both positively and negatively charged carriers injected from the anode and cathode electrodes into solid dielectric material apparently dominate space charge formation phenomena. Some efforts have been conducted on understanding of the steady state flow of charge inside homogenous solid dielectric material under conditions controlled by space charge [29-31]. Figure 5(a) shows the variations of electron density as a function of position (z) from the cathode at different moments of time.

The transport of holes inside polymeric materials can only occurred via electron vacancies within or closely associated with the valence band. So, it is consequently confined to polymer chains and continuous movement of holes requires inter chain hole transfer via tunneling between closely adjacent polymer chains including chains in amorphous regions. Therefore, hole conduction process is more sensitive to morphology of polyethylene.

The variations of hole density as a function of position (z) from the cathode at different moments of time are shown in the Figure 6(a). A relative reduction in electron density is clear at around z = 0.27 mm at all moments of time, i.e. 5.5×10^{19} m^{-3}, 7.11×10^{19} m^{-3} and 1.02×10^{20} m^{-3} at t = 4000 s, 5000 s and 10000 s, respectively. These reductions occur in the hole densities of 7.107×10^{18} m^{-3}, 7.78×10^{18} m^{-3} and 5.93×10^{18} m^{-3} at the above mentioned time moments. This is due to that the electric field (Figure 2) around this position reaches to its minimum, and consequently, ionization rate in the bulk of solid dielectric material reduces. The electron and hole densities show higher number of electron and hole at positions close to the both electrodes, which is due to higher ionization rate of traps close to the anode and cathode electrodes. The spatial variations of space charge densities are in agreement with the performed measurements by Fleming [32].

They selected a Low Density Polyethylene (LDPE) as an insulating material in 225 kV and measured space charge profiles in double laminate layers based on LDPE. His measurements were recorded in short circuit using the Pulsed Electro Acoustic (PEA) method.

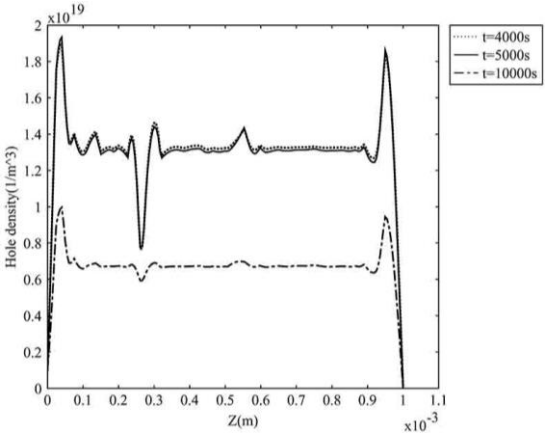

(a)

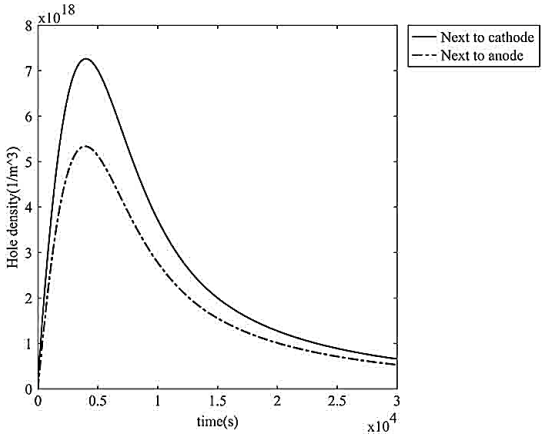

(b)

Figure 6. Hole density in the PE obtained from the simulations for a 1 mm sample, (a) versus distance from the cathode at different moments of time and, (b) versus time at the positions close to cathode (r = 0, z = 0.01 mm) and anode (r = 0, z = 0.99 mm) after voltage application

As shown in Figures 5(b) and 6(b), the densities of electrons and holes next to the anode are a little lower than the cathode. This is, as seen in Figure 2, due to slightly higher electric field in the anode regions compared to cathode region that causes drift of charged particles to the anode more quickly than cathode. The electron density at the positions next to cathode (r = 0, z = 0.01 mm) and anode (r = 0, z = 0.99 mm) peaks almost at t = 8880 s and the corresponding peak values are 6.73×10^{19} m^{-3} and 4.77×10^{19} m^{-3}, respectively.

The peak values of hole density next to cathode and anode with peak values of 7.26×10^{18} m^{-3}, 5.38×10^{18} m^{-3}, almost occurs at t = 3990 s. While as seen in these figures, holes density peaks earlier than electron density, both charged carriers are almost depleted at the same time. Moreover, the density of electrons is more than holes, which is due to higher number of negatively charged carriers injected from the anode and cathode electrodes into solid dielectric material.

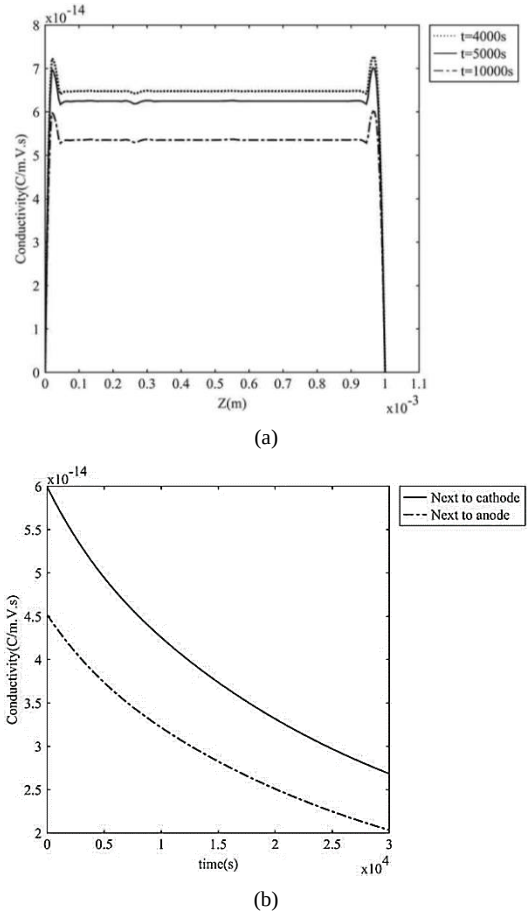

Figure 7. Conductivity in the PE obtained from the simulations for a 1 mm sample, (a) versus distance from the cathode at different moments of time and, (b) versus time at the positions close to cathode (r = 0, z = 0.01 mm) and anode (r = 0, z = 0.99 mm) after voltage application

The effective conductivity of solid dielectric material ($\sigma = e\,(\mu_e\,(n_e + n_{et}) + \mu_h\,(n_h + n_{ht}))$) is shown in Figure 7(a) as a function of position (z) from the cathode at different moments of time. As may be seen, the conductivity within the solid dielectric almost remains constant, except for those regions close to the cathode and anode electrodes. This is due to the higher amount of charged carriers near the electrodes. At t = 4000 s, t = 5000 s and t = 10000 s, the corresponding values for conductivity next to the cathode are 7.225×10^{-14} C/m.V.s, 6.970×10^{-14} C/m.V.s and 5.942×10^{-14} C/m.V.s which slightly lower than that next to the anode, i.e. 7.274×10^{-14} C/m.V.s, 7.016×10^{-14} C/m.V.s and 6.014×10^{-14} C/m.V.s.

This is due to slightly lower amount of charged carriers next to the anode electrode (Figures 5 and 6). As was mentioned before, this is due to slightly lower field in the positions near to the cathode electrode, which results in the drift of charged particles to the cathode electrode slower than anode electrode. As time progresses, conductivity begins to be affected by the removal of charged carries within solid dielectric material, and consequently decreases. At greater distances from the cathode, conductivity is enhanced as well. Figure 7(b) shows the effective conductivity of solid dielectric material as a function of time at the positions next to cathode (r = 0, z = 0.01 mm) and anode (r = 0, z = 0.99 mm).

The conductivity next to the anode after 30000 s of voltage application (σ_f) is reduced to 45% of its initial value, σ_i, and to 44% for next to the cathode. Thus, the drop in conductivity over the period of the voltage application ($\Delta\sigma = \sigma_i - \sigma_f$) close to the cathode is a little higher than anode. This can be due that the electric field (Figure 2) in the regions near to the cathode is a little higher than the region near to the anode in the bulk of solid dielectric material. Serdyuk et al observed a similar decrease in effective conductivity with time in modeling of a dielectric slab of 100 μm length after a voltage application [11].

Figure 8 shows the evolution with time of the number density of electrons, holes, trapped electrons and trapped holes resident in the bulk of solid dielectric material. It may be seen that for every species, the trapped ones are more numerous and remain longer within the solid dielectric. The density of the trapped electrons (n_{et}) after 30000 s of voltage application is reduced to 42% of its initial value, while to 43% for trapped holes (n_{ht}).

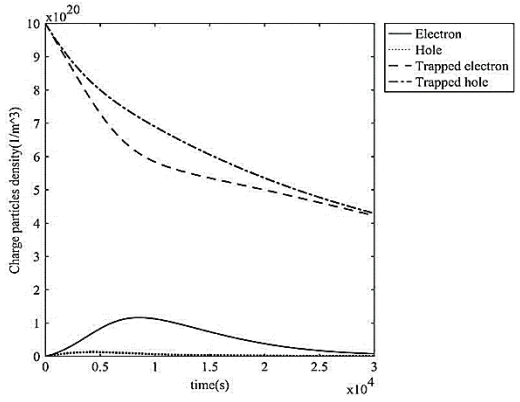

Figure 8. Time history of number density of different spices in solid dielectric material as a function of time at r = 0 and z = 0.22 mm

Thus, over the period of the voltage application, the drop in density of trapped electrons in the middle of dielectric slab is a little higher than trapped holes. As seen in the Figure 8, electrons and holes peak at respectively at t = 8880 s and 3990 s and leave the bulk of dielectric

material quickly (within 25000 s). On the other hand, the trapped ones linger for such a long time. This is obviously due to that the trapped ones remain in deep traps.

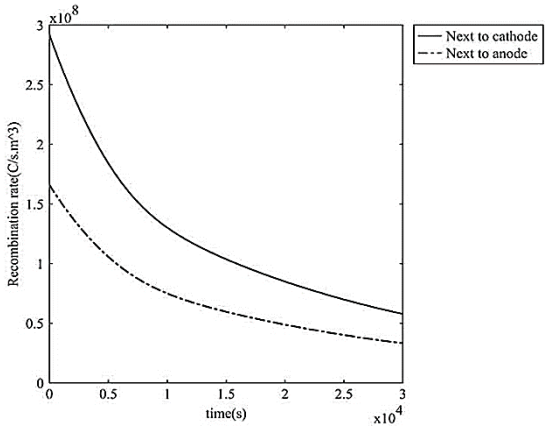

Figure 9. Time history of recombination rate in solid dielectric materials as a function of time at different positions from the cathode after voltage application

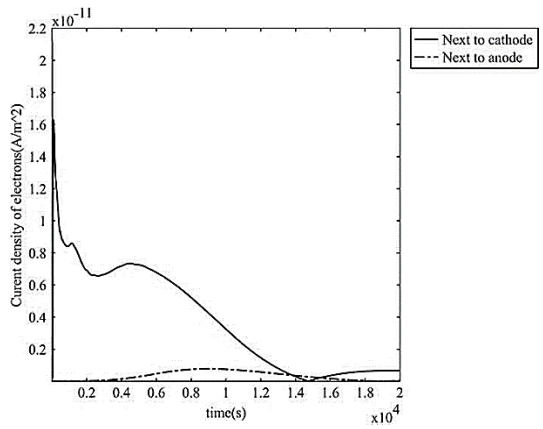

(a)

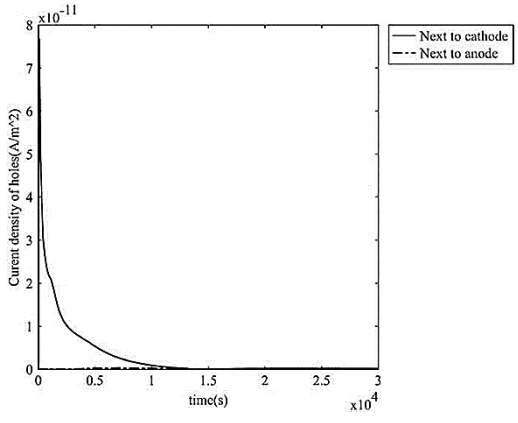

(b)

Figure 10. Time history of current density of, (a) Electrons and, (b) Holes as a function of time at different points along z-axis

In this study, charged carriers recombination is introduced to explain electroluminescence phenomena in bulk of solid dielectric material. The total recombination rate due to different kinds of carriers is presented in the Figure 9 as a function of time at different positions from the cathode. As seen, recombination rate next to cathode after 30000 s of voltage application is reduced to 19% of its initial value, and to 20% for next to cathode. Reduction in the charged carriers (Figure 8) results in reduction of recombination. As seen, the recombination rate is mainly governed by trapped carriers rather than free carriers. It must be noted that there is a difference between recombination rate and luminescence yield. First, every recombination event does not necessarily result in luminescence yield. Secondly, the light emission does not necessarily originate from recombination processes [33].

The flow of current in dielectric insulators and the associated space charge effects are topics of considerable technical interest. As is shown in Figure 10, at positions along z-axis next to the anode and cathode, the electrons and holes current densities reach a maximum value soon after the number of electrons (Figure 5). In addition, holes in the bulk of the solid dielectric material (Figure 6) reach to their peak values, followed by a decrease and reaching to a quasi equilibrium state.

The peak values of current density of electrons and holes next to the anode and cathode occur nearly at t = 8880 s and t = 15 s, respectively. As shown, owing to higher electric field at the positions near to cathode in the bulk of solid dielectric material (Figure 2) and higher number of charged species in this region (Figures 5, 6), the maximum current density of electrons next to cathode is almost 27 times higher than that next to anode.

It shows that the maximum value of current density of holes next to the cathode is more than 1000 times higher than that next the anode. The presence of trapped charges inside the bulk of dielectric material seems to fasten the setup of quasi equilibrium for the current. Moreover, these results indicate different variations in the dominant mechanism of the charging current at different points along z-axis. The variations in the current densities (electrons and holes) are higher at positions nearer to the cathode, evidently due to slightly higher amount of density of charged carriers in this region (Figures 2, 5 and 6).

The temporal behavior of current density corroborates the experimental findings by Chen et al. [34]. They measured the current and space charge distribution simultaneously in cross linked polyethylene sample [35]. They observed multi current peaks at high fields. They showed that the different components of current density generally follow a decent trend [36]. So, they were expected that it should be from a response of dielectric to a dc voltage application. Their findings show that there are transient current peaks occurring within the first moments of time after the application of dc voltage.

Moreover, they have stated that at the same time there are significant developments in space charge movement within the material. The experimental findings of Roy et al. [10] show only decreasing from their initial values along with the steady-state oscillations. Adamec et al. concluded that a weak polarization mechanism in polyethylene is dominant at short times and is a function of applied field [37]. Therefore, decreasing part of these curves corresponds to transport of charges (Figure 8).

Figures 11(a) and 11(b) show the increasing effects of applied voltage on the peak values of different components of current density (electrons and holes) in solid dielectric material at three different temperature values. The simulations are performed for the operating parameters presented in Table 1, except for the applied electric field, which is varied between 5 kV/mm and 100 kV/mm. As seen in these figures, at T = 273 K, T = 293 K and T = 300 K, the electron current density at the applied field of E_a = 100 kV/mm are respectively 6, 6.3 and 144 times higher than that at the applied field of E_a = 5 kV/mm.

These ratios for hole density are 7.4, 6 and 435, respectively. These findings corroborate with the experimental results by Lee et al. [22]. They studied the space charge behavior such as charge distribution and electrical conduction of maleic anhydride grafted LDPE. They observed that at higher temperatures and electric fields, the current densities are higher. Moreover, the lower applied electric fields (below 50 kV/mm) do not enhance the peak values of different components of current density significantly.

Moreover, these obtained results corroborate computational and experimental results reported by Roy et al. [10]. The enormous increase in the current density of electrons and holes at higher temperatures is due to very large effects of higher temperatures on the injection of charged carriers into solid dielectric material from anode and cathode electrodes based of Schottky's law, which is represented in Equations (10) and (11).

These behaviors versus temperature variations are in agreement with the observed experimental results by Zhou et al. [28]. Their findings show that the space charge density continually increases with the increase of temperature. They performed their experiments under the same aging time. They concluded that the raising temperature promotes the electrode injecting charge.

The effect of the length of the solid insulating material on the current density and its components looks to be an interesting study. As the length of the solid dielectric increases, for a given temperature, the residence time of charged particles inside the solid insulator is higher. Each electron suffers a larger number of ionizing collisions as it travels from the cathode to the anode, as a result, the production of charged carriers inside the solid insulator is much higher at higher lengths.

Then, it causes increase in current density of electrons and holes and consequently the total current density inside solid insulator. As seen in Figure 12, while the applied electric field across the solid dielectric material is held constant at E = 10 kV/mm. With variation in the length of the solid insulator from 0.1 mm to 5 mm, the current density varies from 1.33×10^{-11} A/m^2 to 8.99×10^{-9} A/m^2 for electrons, 5.25×10^{-12} A/m^2 to 3.83×10^{-9} A/m^2 for holes and 2.24×10^{-11} A/m^2 to 2.30×10^{-8} A/m^2 for total current, respectively. They show that the electron, hole and total current densities at the length of S_z = 5 mm are respectively 676, 730 and 1026 times higher than that at the length of S_z = 0.1 mm.

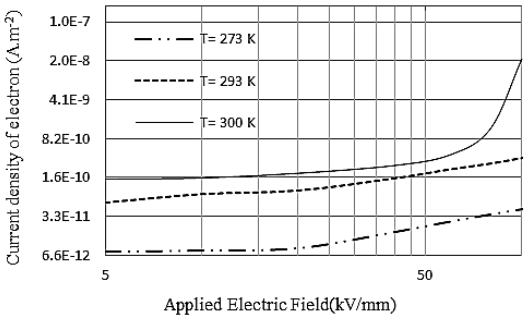

(a)

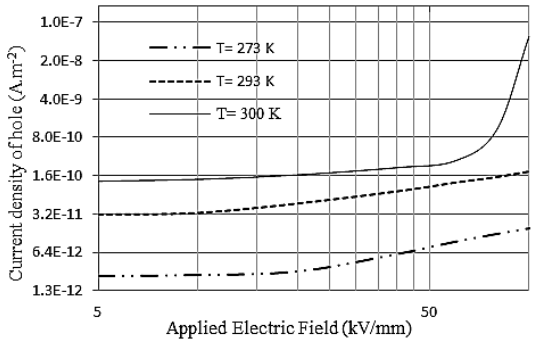

(b)

Figure 11. Variation with applied voltage of the peak values of,
(a) The current density of electrons and,
(b) The current density of holes for different temperatures

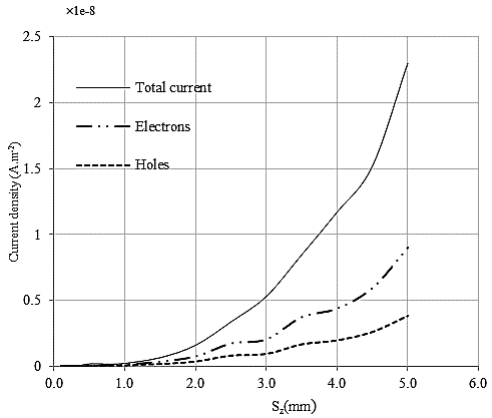

Figure 12. Variation with length of dielectric insulator of the peak values of the current density corresponding to electrons, holes and total current

IV. CONCLUSIONS

A powerful stabilized finite element method has been successfully applied to study the spatio temporal characteristics of charge transfer within solid insulating materials via solving of the governing equations obtained from a two dimensional axisymmetric model. This model was developed for description of space charge including drift, diffusion, and source terms where steep variations of particle densities occur and space charge effect become dominant. As was seen, after voltage application, there is a decrease in electric field along z-axis next to the cathode, which is followed by an increase next to the anode at the all moments of time.

The effect of electric field on the net charge density is higher at positions nearer to the anode. Moreover, our results showed that the variation of electric potential across

the solid dielectric material follows the variation of electric field. It was seen that the electron and hole densities are higher at positions close to the both electrodes. Moreover, the density of electrons is more than holes. In addition, this investigation confirms that the conductivity of a sample of solid dielectric material under applied electric field decreases over time.

It was found that trapped carriers rather than free carriers mainly govern recombination rate. The maximum current density of electrons and holes next to the cathode is much higher than that next to the anode. Moreover, the variations in the current densities (electrons and holes) are higher at positions nearer to the cathode. There is an enormous increase in the current density of electrons and holes at higher temperatures. It was seen that at the lower applied electric fields, peak values of different components of current density are not enhanced significantly.

NOMENCLATURES

μ_b: Band mobility's
$D_{e,h}$: Diffusion coefficient
R_{eht}, R_{eth}, R_{eh}, R_{etht}: Recombination coefficients
T_e, T_h: Trapping coefficients
v: Attempt to escape frequency
φ_c, φ_a: Barrier height for injection
ε_r: Material dielectric constant
T: Temperature
S_z: Sample length
E_a: Applied Electric Field

ACKNOWLEDGEMENTS

The authors would like to acknowledge Institute for Science and High Technology and Environmental Sciences for financial support within the project 1.140-90/2/24.

REFERENCES

[1] G. Shahgholian, "Review of Power System Stabilizer - Application, Modeling, Analysis and Control Strategy", International Organization on Technical and Physical Problems of Engineering (IJTPE), Issue 16, Vol. 5, No. 3, pp. 41-52, September 2013.

[2] M. Rashidi, M. Kalantar, S. Hosseinzadeh, N. Samsunchi, A. Kazemi, "Modeling of Line Parameters for the Broadband Power Line Carrier Channel", International Organization on Technical and Physical Problems of Engineering (IJTPE), Issue 9, Vol. 3, No. 4, pp. 132-136, December 2011.

[3] S.L. Roy, H. Miyake, Y. Tanaka, T. Takada, G. Teyssedre, C. Laurent, "Simultaneous Measurements of Electroluminescence and Space Charge Distribution in Low Density Polyethylene Under a Uniform DC Field", Jour. of Phys. D: Appl. Phys., Vol. 38, pp. 89-94, 2005.

[4] J.C. Fothergill, L.A. Dissado, "Space Charge in Solid Dielectrics", the Dielectrics Society, 1998.

[5] L.A. Dissado, G. Mazzanti, G.C. Montanari, "Role of Trapped Space Charges in Electrical Aging of Insulating Materials", IEEE TDEI, Vol. 4, No. 5, pp. 496-596, 1997.

[6] H.J. Wintle, "Discharge Currents Following Space Charge Limited Current Conditions in Insulators", Jour. Appl. Phys., Vol. 62, pp. 2933-2936, 1987.

[7] P.A. Torpey, ''Double-Carrier Injection and Recombination in Insulators, Including Diffusion Effects", J. Appl. Phys., Vol. 56, pp. 2284-2294, 1984.

[8] K.K. Thornber, D.F. Nelson, J.A. Cooper, "Cube Root Broadening of Surface Charge Packets", Appl. Phys. Letters, Vol. 39, pp. 843-845, 1981.

[9] H.J. Wintle, "The Discharge of Charged Dipolar Insulating Materials", Jour. Appl. Phys., Vol. 63, pp. 1705-1713, 1988.

[10] S.L. Roy, G. Teyssedre, C. Laurent, "Numerical Methods in the Simulation of Charge Transport in Solid Dielectrics", IEEE, Vol. 13, No. 2, pp. 239-246, 2006.

[11] Y.V. Serdyuk, S.M. Gubanski, "Computer Modeling of Interaction of Gas Discharge Plasma with Solid Dielectric Barriers", IEEE TDEI, Vol. 12, No. 4, pp. 725-735, 2005.

[12] I. Christie, D. Griffith, A. Mitchell, O. Zienkiewicz, "Finite Element Methods for Second Order Differential Equations with Significant First Derivatives", Int. Jour. Numer. Meth. Eng., Vol. 10, pp. 1389-1396, 1976.

[13] J. Heinrich, P. Huyakorn, O. Zienkiewicz, A. Mitchell, "An Upwind Finite Element Scheme for Two Dimensional Convective Transport Equation", Int. Jour. Numer. Meth. Eng., Vol. 11, pp. 131-143, 1977.

[14] J. Heinrich, O. Zienkiewicz, "Quadratic Finite Element Schemes for Two-Dimensional Convective Transport Problems", Int. Jour. Numer. Meth. Eng., Vol. 11, pp. 1831-1844, 1977.

[15] H.J. Wintle, "Charge Motion in Technical Insulators - Facts, Fancies and Simulations", IEEE TDEI, Vol. 10, No. 5, pp. 826-841, 2003.

[16] R.W. Hockney, J.W. Eastwood, "Computer Simulation Using Particles", Hilger, Bristol, 1988.

[17] S.K. Doss, K.A. Miller, "Dynamic ADI Methods for Elliptic Equations", Siam. Jour. Numer. Anal., Vol. 16, pp. 837-856, 1979.

[18] D.W. Hewett, D.J. Larson, S.K. Doss, "Solution of Simultaneous Partial Differential Equations Using Dynamic ADI - Solution of the Streamlined Darwin Field Equations", Jour. Comput. Phys., Vol. 101, No. 11, pp. 11-24, 1992.

[19] V. Vahedi, G. DiPeso, "Simultaneous Potential and Circuit Solution for Two-Dimensional Bounded Plasma Simulation Codes", Jour. Comput. Phys., Vol. 131, pp. 149-163, 1997.

[20] D. Scharfetter, H. Gummel, "High Injection in Epitaxial Transistors", IEEE Trans. Elec. Dev., Vol. 16, pp. 245-252, 1969.

[21] M.M. Becker, D. Loffhagen, W. Schmidt, "A Stabilized Finite Element Method for Modeling of Gas Discharges", Computer Physics Communications, Vol. 180, pp. 1230-1241, 2009.

[22] S.H. Lee, J.K. Park, "Space Charge and Electrical Conduction in Maleic Anhydride Grafted Polyethylene", IEEE TDEI, Vol. 2, No. 6, pp. 1132-1139, 1995.

[23] J.M. Alison, "A High Field Pulsed Electro Acoustic Apparatus for Space Charge and External Circuit Current Measurement within Solid Insulators", Meas. Sci. Technol., Vol. 9, pp. 1737-1750, 1998.

[24] T. Takada, "Acoustic and Optical Methods for Measuring Electric Charge Distributions in Dielectrics", Conference on Electrical Insulation and Dielectric Phenomena, Austin, TX, USA, 17-20 Oct. 1999.
[25] H.J. Wintle, "Charge Motion in Technical Insulators, Facts, Fancies and Simulations", Vol. 10, No. 5, pp. 826-841, 2003.
[26] J.L. Auge, C. Laurent, D. Fabiani, G.C. Montanari, "Investigating DC Polyethylene Threshold by Space Charge - Current & Electroluminescence Measurements", IEEE TDEI, Vol. 7, No. 6, pp. 797-803, 2000.
[27] N. Hozumi, G. Teyssedre, C. Laurent, K. Fukunaga, "Investigating Electroluminescence Excitation by Space Charge Measurements under Transient Stress in Cross Linked Polyethylene", Intentional Conference on Solid Dielectrics, Toulouse, France, 5-9 July 2004.
[28] L.R. Zhou, G.N. Wu, B. Gao, K. Zhou, J. Liu, K.J. Cao, L.J. Zhou, "Study on Charge Transport Mechanism & Space Charge Characteristics of Polyimide Films", IEEE TDEI, Vol. 16, No. 4, pp. 1143-1149, 2009.
[29] N.F. Mott, R.W. Gurney, "Electronic Processes in Ionic Crystals", Oxford University Press, New York, p. 42, 1940.
[30] A. Rose, "Space Charge Limited Currents in Solids", Phys. Rev., Vol. 97, pp. 1538-1544, 1955.
[31] M.A. Lampert, P. Mark, "Current Injection in Solids", Academic, New York, 1970.
[32] R.J. Fleming, "Space Charge in Polymers, Particularly Polyethylene", Brazilian Journal of Physics, Vol. 29, No. 2, pp. 280-294, 1999.
[33] F. Baudoin, D.H. Mills, P.L. Lewin, S.L. Roy, G. Teyssedre, C. Laurent, "Modeling Electroluminescence in Insulating Polymers under AC Stress - Effect of Excitation Waveform", Jour. Phys. D: Appl. Phys., Vol. 44, pp. 165402-165417, 2011.
[34] G. Chen, T.Y.G. Tay, A.E. Davies, T. Tanaka, T. Takada, "Electrodes and Charge Injection in Low Density Polyethylene - Using the Pulsed Electroacoustic Techniques", IEEE, Vol. 8, No. 6, pp. 867-873, 2001.
[35] G. Chen, "Anomalous Phenomena in Solid Dielectrics under High Electric Fields", International Conference on Properties and applications Dielectric Materials, Harbin, China, 19-23 July 2001.
[36] G. Chen, Z. Xu, "Charge Trapping and De-Trapping in Polymeric Materials", Jour. Appl. Phys., Vol. 107, pp. 1237072009-1-5, 2009.
[37] V. Adamec, J.H. Calderwood, "The Significance of Dipolar Mechanisms in Relation to Charge and Discharge Currents in Polyethylene", Jour. Phys. Appl. Phys., Vol. 16, pp. 203-211, 1983.

BIOGRAPHIES

Alireza Ganjovi received his Ph.D. degree in the field of Gaseous Discharges in Electrical Engineering Department at the Indian Institute of Technology (IIT), Kanpur, India, 2011. He is currently Faculty Member of Photonics Research Institute in the Graduate University of Advanced Technology, Kerman, Iran. His research interests are applications of plasma physics and numerical modeling of gaseous discharges.

Saeedeh Khezripour received her M.Sc. degree in the field of Solid State Physics in Physics Department at the Iran University of Science and Technology, Tehran, Iran, in 2011. She is currently Ph.D. student in Physics (Atomic and Molecular Physics) at the Graduate University of Advanced Technology, Kerman, Iran. Her research interests are nanostructure semiconductors, gas discharge, quantum dots.